INDIAN JOURNAL OF SCIENCE AND TECHNOLOGY

ORIGINAL ARTICLE

# Anti-Angiogenic Properties of Silver Nanoparticles Synthesized from *Clerodendrum schmidtii* Leaf Extract

**Allan S Domencil[1], Sharon E Lazaro[1,2], Cesar V Ortinero[2,3], Danila S Paragas[1,2]***

**1** Department of Chemistry, College of Science, Central Luzon State University, Science City of Muñoz, Nueva Ecija, Philippines
**2** Nanotechnology R&D Facility, Central Luzon State University, Science City of Muñoz, Nueva Ecija, Philippines
**3** Department of Environmental Science, College of Science, Central Luzon State University, Science City of Muñoz, Nueva Ecija, Philippines

OPEN ACCESS

**Received:** 01/09/2025
**Accepted:** 27/11/2025
**Published:** 31/12/2025

**Citation:** Domencil AS, Lazaro SE, Ortinero CV, Paragas DS (2025) Anti-Angiogenic Properties of Silver Nanoparticles Synthesized from *Clerodendrum schmidtii* Leaf Extract. Indian Journal of Science and Technology 18(48): 3946-3956. https://doi.org/10.17485/IJST/v18i48.1531

* **Corresponding author**.

danilaparagas1010@clsu.edu.ph

**Funding:** None

**Competing Interests:** None



Published By Indian Society for Education and Environment (iSee)

**ISSN**
Print: 0974-6846
Electronic: 0974-5645

## Abstract

**Objectives:** This study aimed to synthesize silver nanoparticles (AgNPs) using ethanol leaf extracts of *Clerodendrum schmidtii* and to evaluate their anti-angiogenic activity as a potential basis for cancer-related applications.

**Methods:** Freeze-dried leaves were extracted with ethanol, and AgNPs were synthesized under optimized conditions (1:1 extract-to-$AgNO_3$ ratio, pH 11, 80 °C, 30 min). The resulting nanoparticles were characterized using ultraviolet-visible (UV-Vis) spectrophotometry, Fourier-transform infrared (FTIR) spectroscopy, scanning electron microscopy (SEM), dynamic light scattering (DLS), and zeta potential analysis. Anti-angiogenic activity was assessed using the chorioallantoic membrane (CAM) assay with proper controls and replication.

**Findings:** The CS-AgNPs had an average particle size of 54.3 $\pm$ 15.7 nm and a zeta potential of -77.6 $\pm$ 6.6 mV, indicating excellent colloidal stability. UV-Vis analysis showed a peak at 403 nm. The FTIR analysis revealed the functional groups (-OH, C=O, C=C, C-N) associated with phytochemical-mediated reduction and capping. SEM analysis showed predominantly spherical particles. In the CAM assay, CS-AgNPs produced a dose-dependent inhibition of angiogenesis, reaching a 73.78 $\pm$ 2.34% reduction in vascular branching at 500 ppm extract equivalent (50 ppm AgNPs). This inhibitory effect was significantly greater than the 54.71 $\pm$ 3.31% inhibition observed with the crude extract alone. Nonlinear regression confirmed an $IC_{50}$ of 249.4 $\pm$ 7.7 ppm.

**Novelty:** This study reports, for the first time, the green synthesis of AgNPs using *C. schmidtii* and demonstrates their significant anti-angiogenic activity, highlighting their potential as plant-derived candidates for anticancer nanomedicine, pending further *in vivo* validation.

**Keywords:** *Clerodendrum schmidtii*; Silver Nanoparticles; Green Synthesis; Anti-angiogenic Activity; Chorioallantoic Membrane Assay; Dose-dependent Inhibition

# 1 Introduction

Plants are a rich source of bioactive metabolites with diverse therapeutic applications, and many plant-derived compounds have shown promise in cancer treatment due to their lower toxicity and synergistic biochemical activities [1]. Cancer remains a major global health burden, ranking as the second leading cause of mortality worldwide [2] and the third in the Philippines, where more than 63,000 deaths were recorded in 2022 [3]. Although conventional therapies exist, issues such as high cost, adverse effects, and limited accessibility highlight the need for safer and more affordable treatment alternatives, including plant-based approaches [4].

Nanotechnology has advanced this search by enabling the development of biocompatible nanomaterials for drug delivery, imaging, and anticancer applications [5]. Plant-mediated ("green") synthesis of silver nanoparticles (AgNPs) has emerged as an eco-friendly and cost-effective alternative to chemical synthesis, yielding nanoparticles with established cytotoxic, antimicrobial, and anti-angiogenic properties [6].

Numerous medicinal plants, including *Trachyspermum ammi* [7], *Musa acuminata colla* [8], *Aegle marmelos, Eugenia jambolana* and *Annona muricata* [9], have been explored for AgNP biosynthesis, demonstrating significant anticancer and anti-angiogenic activities across various models. However, despite these advances, the therapeutic potential of many biologically rich but understudied plant species remains unexplored.

One such species is *Clerodendrum schmidtii* C.B. Clarke, an ornamental plant native to Southeast Asia and was reported to be used in gynecologic medicine of the Himalayan region [10]. While several members of the *Clerodendrum* genus (e.g. *C. inerme, C. chinense, C. thomsoniae*) exhibit anti-cancer or anti-angiogenic activities, no studies to date have characterized the phytochemical properties or biomedical potential of *C. schmidtii*. Moreover, there are no published reports on the green synthesis of AgNPs using *C. schmidtii*, nor on its ability to modulate angiogenesis, a key process involved in tumor growth and metastasis.

This knowledge gap presents an opportunity to identify a novel plant-based candidate with potentially unique reducing and stabilizing biomolecules capable of producing state nanoparticles with therapeutic relevance. Establishing *C. schmidtii* as a viable biofactory for nanoparticle synthesis could broaden the phytochemical diversity represented in green nanotechnology and reveal new angiogenic agents of value for cancer research.

Therefore, this study reports for the first time the green synthesis of AgNPs using *C. schmidtii* leaf extract (CS-AgNPs) and evaluates their anti-angiogenic activity using the chorioallantoic membrane (CAM) assay. By optimizing synthesis conditions and characterizing the resulting nanoparticles, this work aims to (1) introduce *C. schmidtii* as a novel plant source for AgNP fabrication, (2) provide the first evidence of its anti-angiogenic activity, and (3) contribute new knowledge to the development of plant-based nanotherapeutics.

# 2 Methodology

## 2.1 Chemicals and Reagents

The following analytical-grade chemicals and reagents were used in this study: Ethanol (95%), analytical grade (Univar - Ajax Finechem), Silver nitrate ($AgNO_3$), analytical grade (Techno Pharmachem, India), Deionized water, laboratory-produced using Nano Filtration System ((Model W3T324337, Evoqua Water Technologies GmbH, Germany), Phosphate-buffered saline (PBS), pH 7.4 (Techno Pharmachem, India), Ethanol (70%) for egg surface sterilization (Univar - Ajax Finechem), and Whatman No. 1 filter paper (Cytiva/Whatman, UK).

## 2.2 Instruments and Equipment

The instruments used for sample preparation, nanoparticle synthesis, and characterization were as follows: Freeze Dryer (Labtron LFFD-A10; Labtron Equipment Ltd., UK); Mechanical Grinder (Retsch ZM200; Retsch GmbH, Germany); Rotary Evaporator (DLAB RE100-Pro; DLAB Scientific, China); Drying Oven (Memmert UM400; Memmert GmbH, Germany); UV-Visible Spectrophotometer (Hitachi UH5300; Hitachi High-Tech, Japan); Dynamic Light Scattering and Zeta Potential Analyzer (Horiba nanoPartica SZ-100; HORIBA Scientific, Japan); Scanning Electron Microscope (SEM) (Hitachi SU3800; Hitachi High-Tech, Japan); Fourier-Transform Infrared Spectrometer (FTIR) (PerkinElmer Spectrum Two; PerkinElmer Inc., USA); Incubator for egg development (Quincy Lab Incubator (Model 12-140E, Quincy Lab Inc., Chicago, IL, USA)); and Sterile filter discs, 5 mm diameter (manufacturer not specified).

## 2.3 Sample Collection and Preparation

The leaves of *C. schmidtii* were collected in Science City of Muñoz, Nueva Ecija, Philippines. The plant was authenticated by the Department of Biological Sciences, College of Science, Central Luzon State University, Science City of Muñoz. Fresh leaves were cleaned by gentle rinsing with tap water followed by deionized water, then dried with absorbent paper and stored at -20°C before processing[11].

The leaves were freeze-dried until constant weight and ground to 1.0 mm to ensure efficient solvent penetration during extraction. Freeze-drying as a pre-treatment has been shown to preserve thermolabile bioactive compounds and improve extraction efficiency[12]. The dried leaf powder was macerated in 95 % ethanol for 72 h with daily agitation. Maceration is a widely adopted conventional extraction method in which solvents penetrate the plant matrix, solutes dissolve, and they diffuse out into the solvent[13]. The mixture was filtered using Whatman No. 1 filter paper, and the filtrate was concentrated under reduced pressure using a rotary evaporator at 50 °C until a stable mass was obtained. The dried crude extract was transferred to airtight amber containers and stored at 4-7 °C until further use.

A 1000 ppm stock solution of the extract was prepared by dissolving 0.10 g of crude extract in a small portion of deionized water and adjusting the volume to 100 mL in a volumetric flask. The solution was mixed thoroughly and used to prepare working concentrations immediately before analysis.

## 2.4 Synthesis of *Clerodendrum schmidtii*-Silver Nanoparticles (CS-AgNPs)

### *2.4.1. Silver Nitrate Precursor*

A 1.00 mM $AgNO_3$ solution was prepared by dissolving 0.0170 g $AgNO_3$ in deionized water and diluting to 1000 mL. Stored in the dark, the solution was used within one week.

### *2.4.2. Optimization of Phytofabrication Parameters*

Optimization of the silver nanoparticle synthesis was performed before establishing the final procedure. Three major parameters were evaluated: (1) extract-to-silver nitrate ratio, (2) reaction temperature and time, and (3) pH of the reaction mixture. The protocol was adapted from Paragas et al.[14] by modifying the extract-$AgNO_3$ ratio, reaction temperature, and reaction time to optimize synthesis conditions.

To determine the optimal plant extract concentration (1000 ppm) and $AgNO_3$ (1 mM solution), extract-to-$AgNO_3$ ratios of 1:9, 2:8, 3:7, 4:6, and 5:5 (v/v) were prepared Each mixture was stirred at 200 rpm in the dark, and nanoparticle formation was monitored through visual color change and by recording the surface plasmon resonance (SPR) peak at 400-500 nm using UV-Vis spectrophotometry.

The ratio that produced the most intense and well-defined SPR peak was subsequently tested under different thermal conditions. Reaction temperatures of 60 °C, 80 °C, and 100 °C and reaction times of 30, 60, and 90 min were evaluated while keeping all other parameters constant. In a separate set of trials, the initial pH of the optimal extract-$AgNO_3$ mixture was adjusted to 7, 9, and 11 before heating. For each parameter set, nanoparticle formation and peak characteristics ($\lambda_{max}$ position, peak sharpness, and absorbance intensity) were used to assess synthesis efficiency.

Based on these experiments, the combination of extract ratio, temperature, pH, and reaction time that yielded the strongest and narrowest SPR peak, consistent with well-formed and uniformly sized AgNPs, was selected as the optimized condition for the final phytofabrication protocol.

### *2.4.3. Optimized Synthesis Procedure*

For nanoparticle synthesis, the plant extract and $AgNO_3$ were combined at the experimentally determined optimized extract-to-AgNO3 ratio. The mixture was adjusted to the optimal pH, stirred in the dark at 200 rpm, and heated to the optimized reaction temperature for the optimal reaction time, during which the characteristic color transition from pale yellow to reddish-brown indicated AgNP formation. Completion of the reaction was confirmed by the presence of a distinct SPR band at 400-500 nm.

The resulting CS-AgNP dispersion was cooled to room temperature and stored in amber bottles at 4-7 °C until characterization.

### *2.4.4. Characterization of CS-AgNPs*

The synthesized CS-AgNPs were characterized using multiple analytical techniques. UV-Vis spectrophotometry was used to scan the absorption spectrum from 300 to 700 nm to confirm the SPR peak associated with AgNP formation. Dynamic light scattering (DLS) was used to determine particle size distribution and zeta potential; all samples were sonicated for 30 min before

analysis to ensure proper dispersion. Scanning electron microscopy (SEM) was performed to visualize particle morphology and surface features. Fourier-transform infrared spectroscopy (FTIR) was used to identify functional groups from the *C. schmidtii* extract responsible for reducing $Ag^+$ ions and stabilizing the resulting nanoparticles.

## 2.5 Anti-Angiogenic Activity

### *2.5.1. Test Solutions*

The optimized CS-AgNP suspension (containing 500 ppm plant extract and 50 ppm AgNPs) was serially diluted with sterile deionized water to obtain test concentrations of 62.5/6.25 ppm, 125/12.5 ppm, 250/25 ppm, and 500/50 ppm (extract/AgNP, respectively). The crude extract (1000 ppm) was prepared similarly and used as a comparative treatment. All solutions were freshly prepared prior to the assay.

### *2.5.2. Chorioallantoic Membrane (CAM) Assay*

The anti-angiogenic activity was assessed using the chicken chorioallantoic membrane (CAM) assay following Ajaykumar et al.[15], with modifications to ensure consistency and sterility. Fertilized chicken eggs were cleaned with sterile gauze, randomly assigned to each treatment group (n = 3 per group), and incubated at 37 °C with 60-70% relative humidity in a forced-air incubator. Eggs were rotated automatically during the first three days to prevent embryo adhesion.

On Day 5 of incubation, each egg surface was sterilized with 70% ethanol, and a 2 × 2 cm window was created on the air-sac region using a sterile scalpel. The inner membrane was carefully removed to expose the CAM vasculature. Sterile Whatman filter paper discs (5 mm diameter) were saturated with 20-30 $\mu$L of each test solution and gently placed in an area containing first- or second-order CAM blood vessels. Phosphate buffer saline (PBS) served as the negative control.

The window was resealed with sterile parafilm to maintain humidity, and eggs were returned to the incubator for 24 h without rotation.

Before and after treatment, the CAM was photographed at the same magnification and lighting conditions using a digital camera. Vessel density was quantified by manually counting branching points within a defined region of interest (ROI). The percentage reduction in vessel branching was calculated as:

$$\%Vessel\ Reduction = \left(\frac{Branching\ before\ treatment - Branching\ after\ treatment}{Branching\ \ before\ treatment}\right) x\ 100\%$$

### *2.5.3. $IC_{50}$ Determination Using GraphPad Prism*

The concentration of CS-AgNPs required to inhibit 50% of vascular branching ($IC_{50}$) was determined using GraphPad Prism 9.0.0. Percentage inhibition values obtained at 62.5, 125, 250, and 500 ppm were entered as Y-values, with the corresponding nanoparticle concentrations entered as X-values. A nonlinear regression analysis was performed by selecting "Dose-response" and fitting the data to a four-parameter logistic (4PL) model with variable slope [log(inhibitor) vs. response]. X-values were treated as concentrations and automatically log-transformed by the software during model fitting. The $IC_{50}$ value was computed from the fitted curve along with the associated regression parameters. Goodness-of-fit was evaluated using standard Prism diagnostics, and the final $IC_{50}$ value reported is the best-fit estimate from the 4PL model.

### *2.5.4. Statistical Analysis*

Data were expressed as mean ± SD. Differences among treatment groups were analyzed using one-way ANOVA followed by Tuley's post hoc test, with significance accepted at $p < 0.05$.

# 3 Results

## 3.1 Synthesis of Silver Nanoparticles Using *Clerodendrum schmidtii*

All UV-Vis measurements during AgNP synthesis were conducted under identical spectrophotometric conditions, including instrument settings, cuvette type, path length, and blank correction. Each sample was analyzed in triplicate to ensure reproducibility.

### *3.1.1. Optimization of CS-AgNP Synthesis*

***Effect of Extract-to-$AgNO_3$ Ratio:*** The addition of $AgNO_3$ to the crude *C. schmidtii* extract produced an immediate brownish-green coloration, indicating rapid reduction of $Ag^+$ ions and the onset of AgNP formation. This visual change is consistent

with previously reported plant-mediated AgNP syntheses, where phytochemicals such as phenolics, flavonoids and proteins promote instantaneous nucleation and color development through surface plasmon resonance (SPR) effects[16,17]. Among the volume ratios tested (1:9, 2:8, 3:7, 4:6, and 5:5 extract-to-$AgNO_3$), the 5:5 ratio yielded the highest absorbance ($3.026 \pm 0.213$) at 442 nm, significantly greater than the other ratios ($p < 0.05$) except 1:9 (Table 1). The strong, well-defined SPR band at 442 nm at the 5:5 ratio indicates a high density of small, uniformly distributed nanoparticles, as sharper peaks near 420-450 nm are commonly associated with spherical AgNPs in the 10-40 nm size range[18,19].

**Table 1.** Mean Absorbance Values of CS-AgNP Surface Plasmon Resonance (SPR) Under Varying Reaction Parameters

| Ratio, crude extract:$AgNO_3$ (v/v) | Wavelength, nm | Absorbance* | p-values |
|---|---|---|---|
| 1:9 | 454 | $2.579 \pm 0.149^{ab}$ | |
| 2:8 | 454 | $1.103 \pm 0.130^{d}$ | |
| 3:7 | 440 | $1.729 \pm 0.067^{c}$ | 8.95E-07 |
| 4:6 | 454 | $2.188 \pm 0.250^{bc}$ | |
| 5:5 | 442 | $3.026 \pm 0.213^{a}$ | |
| **Temperature, °C (with ratio 5:5 v/v)** | | | |
| 60 | 450 | $2.319 \pm 0.028^{a}$ | |
| 80 | 446 | $2.342 \pm 0.012^{a}$ | 0.7932 |
| 100 | 446 | $2.365 \pm 0.179^{a}$ | |
| **pH (with ratio 5:5 v/v) temperature 80°C)** | | | |
| 7 | 417 | $1.594 \pm 0.058^{c}$ | |
| 9 | 415 | $1.949 \pm 0.056^{b}$ | 8.09E-07 |
| 11 | 415 | $2.080 \pm 0.102^{a}$ | |
| **Reaction Time, mins (ratio: 5:5 v/v, 80°C, pH 11)** | | | |
| 30 | 416 | $2.454 \pm 0.140^{a}$ | |
| 60 | 416 | $2.427 \pm 0.031^{a}$ | 0.0001 |
| 120 | 414 | $2.152 \pm 0.014^{b}$ | |

*Means in each parameter group with the same superscripts are not significant at 5% level using Tukey HSD

The enhanced nanoparticle formation at the 5:5 ratio suggests an optimal balance between the reducing/capping biomolecules in the extract and the available $Ag^+$ ions. At lower extract proportions (1:9 or 2:8), the reducing agents are likely insufficient to fully convert the silver precursor, resulting in slower nucleation or fewer, larger particles with reduced SPR intensity[20]. On the other hand, very high extract content can introduce excess organic matter, which may increase solution turbidity, limiting efficient nucleation despite rapid initial reduction[21]. The non-significant difference between 5:5 and 1:9 ratios suggests that nanoparticle formation proceeds across a relatively broad range of precursor concentrations. However, the equal-volume condition promoted the most efficient reduction and capping environment, thereby maximizing total nanoparticle formation.

***Effect of Temperature:*** The 5:5 ratio was heated at 60 °C, 80 °C, and 100 °C [Table 1]. All heated mixtures turned dark brown, consistent with AgNP formation. UV-Vis spectra showed broad but comparable SPR peaks at 450 nm ($2.319 \pm 0.028$) at 60 °C, 446 nm ($2.342 \pm 0.012$) at 80 °C, and 446 nm ($2.365 \pm 0.179$) at 100 °C. No significant differences were observed in temperatures ($p < 0.05$), suggesting that once energy input exceeds the nucleation threshold, further heating does not markedly affect nanoparticle yield or optical properties[22]. This plateau effect is consistent with reports that temperature mainly accelerates the early reduction kinetics but has minimal impact on final particle characteristics once rapid nucleation has occurred[21]. The slight blue-shift at higher temperatures (80-100 °C) may reflect faster nucleation producing marginally smaller particles, although the differences were too small to reach statistical significance. Among the tested temperatures, 80 °C was chosen as the optimal condition because it produced the smallest deviation, indicating the highest reproducibility in AgNP synthesis.

***Effect of pH:*** The influence of pH was evaluated using the optimized 5:5 ratio. The unadjusted mixture had a pH of 6.5. Adjusting the pH to 7, 9, and 11 did not cause a visible color change at room temperature, indicating that alkaline conditions alone were insufficient to initiate reduction. Upon heating to 80 °C, all solutions turned dark brown. The SPR intensities increased with increasing pH: pH 7 ($1.594 \pm 0.058$) at 417 nm; pH 9 ($1.949 \pm 0.056$) at 415 nm; and pH 11 ($2.080 \pm 0.179$) at 415 nm.

The enhanced absorbance at alkaline pH is consistent with the literature, indicating that higher pH accelerates the reduction of $Ag^+$ by plant-derived biomolecules, thereby promoting the formation of smaller, more uniformly nucleated nanoparticles[23].

This trend aligns with reports that deprotonation of phenolic and flavonoid groups at high pH increases their electron-donating capacity, resulting in faster nucleation and stronger SPR signals [19]. Accordingly, pH 11 was selected as the optimal pH.

***Effect of Reaction Time***: At the optimized ratio and pH, heating for 30, 60, and 120 min was evaluated. The highest absorbance (2.454 ± 0.140 at 416 nm) occurred at 30 min, which was not significantly different from 60 min but significantly higher than at 120 min. Prolonged heating likely promoted partial agglomeration or degradation of reducing agents, decreasing nanoparticle yield. This pattern is consistent with typical green-synthesis kinetics, where rapid initial reduction leads to a higher concentration of nuclei that later tend to aggregate if exposed to extended thermal energy. Similar time-dependent decreases in SPR intensity have been reported in plant-mediated syntheses, where prolonged heating destabilizes capping molecules, allowing particle growth or aggregation [17].

***Final Optimized Conditions:*** The combined optimization steps identified 5:5 extract-to-$AgNO_3$ ratio, pH 11, 80 °C, and 30 min as the best conditions for CS-AgNP synthesis. Under these conditions, the final product exhibited a strong SPR peak at 403 nm with an absorbance of 2.211 [Figure 1], consistent with the reported AgNP absorption range of 400-450 nm. These results align with previous findings that reaction pH and temperature strongly influence the optical response and stability of plant-mediated AgNPs. pH changes alter particle size and SPR peak characteristics, while higher temperatures typically accelerate reduction and shift SPR intensity and position [18–20].

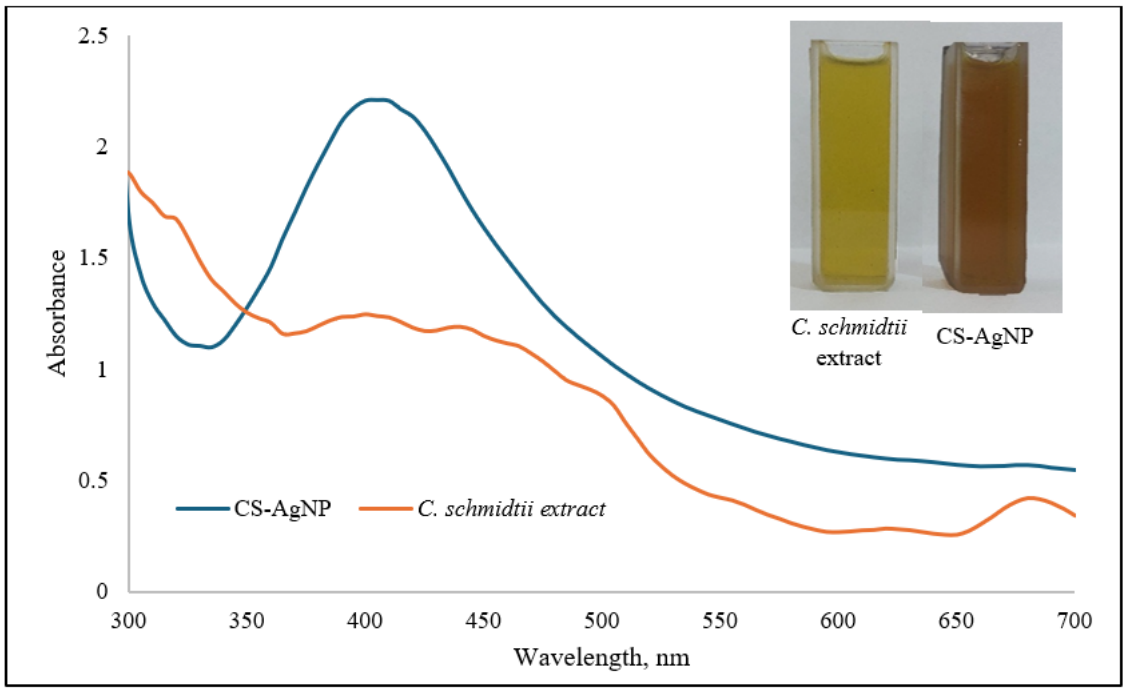


**Fig 1.** The absorbance peak at 403 nm and the brown color signify the biosynthesized CS–AgNPs

The optimized procedure produced a CS-AgNP suspension containing approximately 500 ppm plant extract and a theoretical AgNP concentration of 50 ppm, based on complete reduction of silver nanoparticles [24]. This corresponds to a 5:5 volume ratio of 1000 ppm crude extract to 1.00 mM $AgNO_3$, yielding a final mixture diluted to 500 ppm extract and 50 ppm silver nanoparticles.

### *3.1.2. Characterization of the Synthesized CS-AgNP*

***Particle Size and Zeta Potential:*** Dynamic light scattering analysis revealed that the synthesized CS-AgNP had a mean hydrodynamic diameter of 54.3 ± 15.7 nm, which lies well within the common nanoscale range of 1-100 nm [1]. The colloidal stability of the nanoparticle suspension was evaluated through zeta potential measurements. Nanoparticles with absolute zeta potential values greater than ±30 mV are generally considered stable due to sufficient electrostatic repulsion between particles. The CS-AgNPs have a zeta potential of -77.6 ± 6.6 mV, indicating excellent colloidal stability and minimal tendency to aggregate. The literature similarly reports that absolute zeta potential values exceeding ±60 mV correspond to highly stable colloidal

systems, owing to strong electrostatic repulsion among particles [21]. The pronounced negative surface charge of the CS-AgNPs therefore supports their suitability for further biological and physicochemical applications [25,26].

***Fourier Transform Infrared Spectroscopy (FTIR):*** FTIR spectroscopy was used to identify functional groups in the *C.* schmidtii extracts responsible for reducing $Ag^+$ ions and stabilizing the resulting nanoparticles. Both the crude extract and CS-AgNP spectra exhibited several characteristic peaks. However, noticeable shifts in position and alterations in intensity confirmed chemical interactions between extract biomolecules and silver during nanoparticle formation [Figure 2].

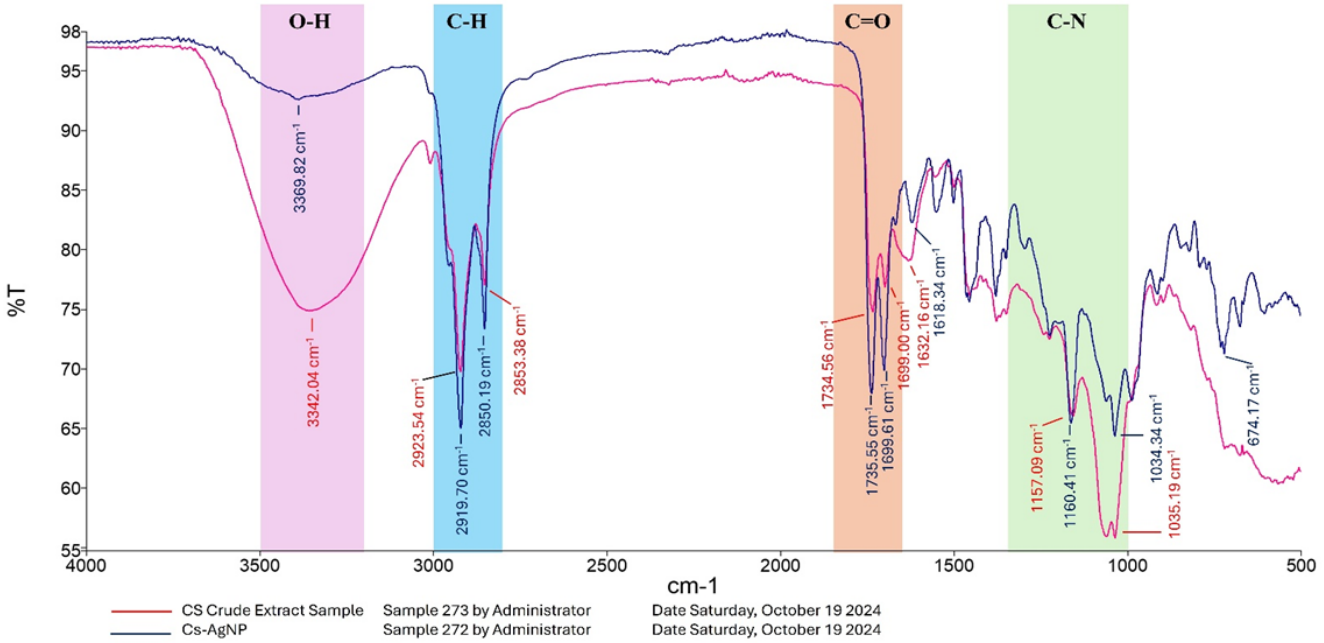


**Fig 2.** FTIR spectra of CS crude extract (red) and CS-AgNPs (blue). The broadening and shifting of peaks indicate interaction of AgNP with the extract

A broad peak at 3342 $cm^{-1}$ in the crude extract, attributed to O-H stretching vibrations, shifted to 3369 $cm^{-1}$ in the CS-AgNP spectrum indicating involvement of hydroxyl-containing compounds in $Ag^+$ reduction. The peak at 2923 $cm^{-1}$, assigned to C-H stretching, showed minimal change after nanoparticle formation.

Carbonyl-associated peaks also shifted: the strong C=O stretching band at 1734 $cm^{-1}$ in the extract appeared at 1699 $cm^{-1}$ in the CS-AgNP spectrum, suggesting partial participation of carbonyl groups in binding or stabilizing the nanoparticles. Similarly, the C=C stretching band shifted from 1632 $cm^{-1}$ to 1618 $cm^{-1}$, further supporting biomolecular interaction. Peaks observed at 1157 $cm^{-1}$ and 1160 $cm^{-1}$ correspond to C-N stretching vibrations, while broadening around 1035 $cm^{-1}$ may be associated with amino-group interactions. The appearance of a new peak at 674 $cm^{-1}$ indicates the formation of an Ag-ligand bond, corroborating the successful capping of the nanoparticles with phytochemicals from the extract. Together, these spectral changes confirm that hydroxyl, carbonyl, amino, and other functional biomolecules served as both reducing and stabilizing agents during green synthesis.

FTIR analysis confirmed involvement of hydroxyl, carbonyl, amino, and C–N functional groups in the reduction and capping of the nanoparticles. The presence of an Ag–ligand band at 674 $cm^{-1}$ further supports phytochemical capping by phenolics/flavonoids and amino-containing biomolecules, as described in previous literature [27].

***Scanning Electron Microscopy:*** SEM analysis revealed that the CS-AgNPs were well distributed across the surface and appeared granular to loosely aggregated at lower magnification (35,000x) (Figure 3). Variations in brightness indicated differences in height, density, or surface charge. At higher magnification (60,000x), the nanoparticles exhibited predominantly spherical to irregular morphologies, which is characteristic of many plant-mediated green syntheses. Such morphological diversity is frequently reported in biosynthesized AgNPs and is typically associated with the heterogeneous nature of plant-derived agents [17].

The SEM findings complement the stability measurements and FTIR results, collectively demonstrating that phytochemicals in the *C. schmidtii* extract functioned effectively as reducing and capping agents. Their involvement contributed to the

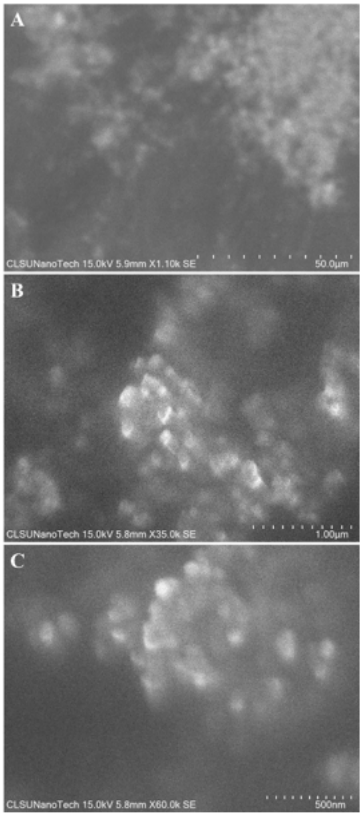


**Fig 3.** SEM image of CS-AgNPs at (A) 1.10K, (B) 35.0K and (C) 60.0K magnifications

uniformity, stability, and morphological integrity of the CS-AgNPs. Taken together, the particle size, zeta potential, FTIR functional signatures, and SEM morphology provide strong evidence of the successful green synthesis of stable, well-dispersed CS-AgNPs. The behavior is consistent with widely reported mechanisms in green-synthesized AgNPs, where plant-derived phenolics, flavonoids, and proteins simultaneously reduce $Ag^{+}$ and stabilize the resulting nanoparticles through surface binding and charge repulsion [19]. Taken together, the particle size, zeta potential, FTIR functional signatures, and SEM morphology provide strong evidence of the successful green synthesis of stable, well-dispersed CS-AgNPs.

## 3.2 Anti-Angiogenic Potential of the Synthesized CS-AgNPs

The anti-angiogenic activity of the synthesized CS-AgNP was evaluated using the CAM assay, with inhibition of vascular branching served as the primary quantitative endpoint (Table 2). Working concentrations of 62.5/6.5, 125/12.5, 250/25, and 500/50 ppm (crude extract/AgNP) were prepared from the CS-AgNP stock solution (500/50 ppm). The crude extract (1000 ppm) served as a comparator, and PBS served as the negative control.

The PBS group showed minimal inhibition ($1.45 \pm 0.52\%$), confirming normal angiogenesis in the absence of treatment. The crude extract produced a moderate inhibition ($54.74 \pm 3.31\%$), indicating the intrinsic anti-angiogenic activity of *C. schmidtii* phytochemicals. CS-AgNPs displayed a clear concentration-dependent response, with inhibition increasing from $5.94 \pm 0.58\%$ at 62.5/6.25 ppm to $73.78 \pm 2.34\%$ at 500/50 ppm, the latter exceeding the crude extract.

Nonlinear regression using a four-parameter logistic (4PL) model yielded an $IC_{50}$ value of $249.4 \pm 7.7$ ppm crude extract equivalent ($24.94 \pm 0.77$ ppm AgNPs), consistent with the observed activity at 250 ppm ($51.62 \pm 1.03\%$). This $IC_{50}$ falls within the range reported for plant-derived AgNPs exhibiting anti-angiogenic effects [17].

Representative CAM images (Figure 4) visually corroborated the quantitative findings. PBS-treated embryos showed a dense, highly organized vascular network (Figure 4A). The crude extract produced moderate vascular suppression (Figure 4B). CS-AgNP-treated CAMs exhibited progressive vascular reduction from mild disruption at 62.5/6.25 ppm (Figure 4C) to substantial

**Table 2.** Inhibition of Angiogenesis by *C. schmidtii* Extract and CS-AgNPs Measured by Percent Reduction in Vascular Branching Points

| Treatment | Concentrations, ppm | | Reduction in Branching Points, %* | p-value |
|---|---|---|---|---|
| | CS | AgNP | | |
| PBS (Control) | - | - | $1.45 \pm 0.52^{d}$ | |
| CS crude extract | 1000 | 0 | $54.71 \pm 3.31^{b}$ | |
| CS-AgNP Low (25%) | 62.5 | 6.25 | $5.94 \pm 0.58^{d}$ | 1.2657E-14 |
| CS-AgNP Moderate (50%) | 125 | 12.5 | $25.93 \pm 1.23^{c}$ | |
| CS-AgNP High (75%) | 250 | 25 | $51.62 \pm 1.03^{b}$ | |
| CS-AgNP Very High (100%) | 500 | 50 | $73.78 \pm 2.34^{a}$ | |

* Means in each parameter group with the same superscripts are not significant at 5% level using Tukey HSD

loss of branching and peripheral vessel thinning at 250/25 ppm (Figure 4E). The highest concentration (500/50 ppm) resulted in pronounced avascular regions and near-collapse of peripheral vessels (Figure 4F), consistent with the most potent inhibition.

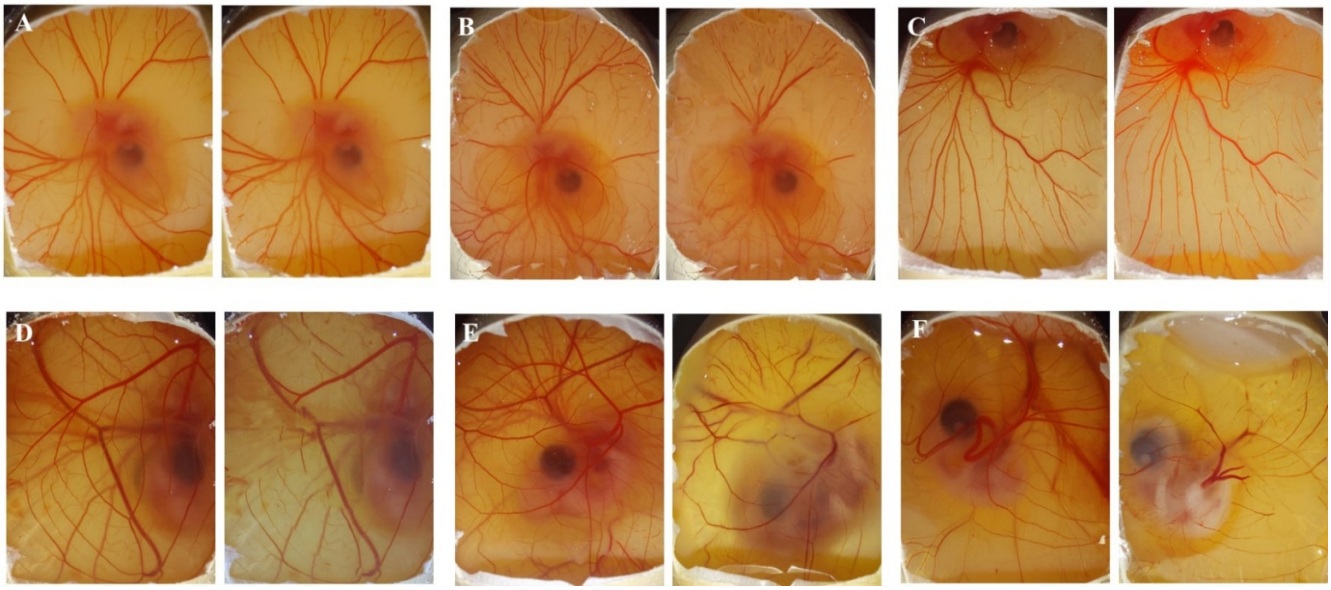


**Fig 4.** Representative CAM images showing dose-dependent anti-angiogenic effects of CS-AgNPs. (A- PBS, B- *C. schmidtii* extract, C- Low CS-AgNP, D- Moderate CS-AgNP, E- High CS-AgNP, F- Very High CS-AgNP)

FTIR analysis suggests that phytochemical capping may contribute to CS-AgNP bioactivity. AgNPs are known to induce reactive oxygen species (ROS), mitochondrial damage, and endothelial apoptosis, which collectively inhibit angiogenesis[28]. Although ROS were not measured directly, the physicochemical characteristics of CS-AgNPs support this mechanism. In particular, the nanoscale size of the particles (54.3 nm) and their phytochemical-derived surface chemistry may enhance their interaction with endothelial cells, as smaller, highly stable nanoparticles with active capping layers are reported to disrupt angiogenic signaling and oxidative stress-mediated vessel regression. For comparison, Bevacizumab (≈149 ppm) induces near-complete inhibition of CAM angiogenesis. Although CS-AgNPs exhibited lower potency, their strong anti-angiogenic activity remains notable for a plant-derived nanomaterial[29].

Although no studies have examined the anti-angiogenic properties of *C. schmidtii*, related species demonstrate relevant biological activities. *C. inerme* exhibits significant antitumor effects in the epidermal growth factor receptor that can treat breast cancer[30]. *C. chinense* extracts and their nanoparticles induce cytotoxicity, apoptosis, mitochondrial disruption, and cell-cycle arrest in breast and cervical cancer cells[31–33]. *C. thomsoniae* also displays strong bioactivity, including antioxidant and antibacterial activity, suppresses DBMA-induced breast tumors, and contains phytochemicals that induce apoptosis[34–36]. These findings suggest that *C. schmidtii* contains bioactive constituents capable of modulating angiogenic pathways.

Overall, CS-AgNPs exhibited strong, dose-dependent anti-angiogenic activity, with the highest concentration outperforming the crude extract. This enhanced effect likely arises from synergism between *C. schmidtii* phytochemicals and silver's nanoscale properties, supporting the potential of CS-AgNPs for further exploration in anti-angiogenic or anticancer applications.

This study, however, is limited by the absence of *in vitro* mechanistic assays and *in vivo* validation. While the CAM assay provides *ex vivo* evidence of dose-dependent anti-angiogenic activity, the specific molecular pathways involved, such as vascular endothelial growth factor (VEGF) modulation, reactive oxygen species (ROS) generation, and endothelial apoptosis, were not directly examined. Future work should therefore include cell-based mechanistic studies and animal models to confirm the biological targets and therapeutic relevance of the CS-AgNPs.

## 4 Conclusion

This study introduces *Clerodendrum schmidtii* as a novel plant source for green synthesis of silver nanoparticles and demonstrates, for the first time, the anti-angiogenic potential of its extract-derived AgNPs. Under optimized conditions, the synthesized CS-AgNPs were stable, well characterized, and predominantly spherical, with phytochemicals functioning as effective reducing and capping agents. The CS-AgNPs exhibited strong dose-dependent inhibition of angiogenesis in the CAM assay, surpassing the activity of the crude extract and confirming their enhanced bioactivity. These findings contribute new knowledge to the field of plant-based nanotherapeutics and highlight *C. schmidtii* as a promising candidate for future development of anti-angiogenic and anticancer nanomaterials.

## 5 Contributory Statement

Conceptualization of the Problem: Allan S. Domencil, Dr. Danila S. Paragas, Experimental Design: Allan S. Domencil, Methodology Development: Allan S. Domencil, Dr. Danila S. Paragas, Data Generation/Investigation: Allan S. Domencil, Data Analysis: Allan S. Domencil, Dr. Danila S. Paragas, Research Guidance/Supervision: Dr. Danila S. Paragas, Dr. Sharon E, Lazaro, Dr. Cesar V. Ortinero, Original Draft Preparation: Allan S. Domencil, Editing & Critical Reviewing: Dr. Danila S. Paragas, Dr. Sharon E. Lazaro, Dr. Cesar V. Ortinero

Note: This study does not involve human testing. All authors affirm that they have substantially contributed to the intellectual content and development of this work

## References


1) Dar RA, Shahnawaz M, Ahanger MA, Majid IU. Exploring the diverse bioactive compounds from medicinal plants: A review. *Journal of Phytopharmacology*. 2023;12(3):189–195. 10.31254/phyto.2023.12307.
2) Organization WH. *Global Health Estimates: Life expectancy and leading causes of death and disability*. 2025. Available from: https://www.who.int/data/gho/data/themes/mortality-and-global-health-estimates.
3) Authority PS. *2022 Causes of deaths in the Philippines (Preliminary as of 28 February 2023)*. 2023. Available from: https://psa.gov.ph/content/2022-causes-deaths-philippines-preliminary-28-february-2023.
4) Haleem A, Javaid M, Singh RP, Rab S, Suman R. Applications of nanotechnology in the medical field: A brief review. *Global Health Journal*. 2023;7(2):70–77. 10.1016/j.glohj.2023.02.008.
5) Kangra K, Kakkar S, Mittal V, Kumar V, Aggarwal N, Chopra H, et al. Incredible use of plant-derived bioactives as anticancer agents. *RSC Advances*. 2025;15(3):1721–1746. 10.1039/d4ra05089d.
6) Soomro R, Abdelmonem M, Meli AD, Panhwar M, Abdullah CAC. A novel plant-based approach for synthesis of iron oxide nanoparticles and cancer therapy. *Discover Chemistry*. 2025;2(1):25. 10.1007/s44371-025-00091-5.
7) Ahmed MJ, Murtaza G, Rashid F, Iqbal J. Eco-friendly green synthesis of silver nanoparticles and their potential applications as antioxidant and anticancer agents. *Drug Development and Industrial Pharmacy*. 2019;45(10):1682–1694. 10.1080/03639045.2019.1656224.
8) Valsalam S, Agastian P, Esmail GA, Ghilan AKM, Al-Dhabi NA, Arasu MV. Biosynthesis of silver and gold nanoparticles using Musa acuminata Colla flower and its pharmaceutical activity against bacteria and anticancer efficacy. *Journal of Photochemistry and Photobiology B: Biology*. 2019;201:111670. 10.1016/j.jphotobiol.2019.111670.
9) Vijayakumar S. Eco-friendly synthesis of gold nanoparticles using fruit extracts and in vitro anticancer studies. *Journal of Saudi Chemical Society*. 2019;23(6):753–761. 10.1016/j.jscs.2018.12.002.
10) Bora KS, Mahamedha. Pharmacognostic standardization and physicochemical analysis of Clerodendrum wallichii (Merr.) leaves. *Pharmaceutical and Biomedical Research*. 2020;5(4). 10.18502/pbr.v5i4.2396.
11) Zygmunt B, Namieśnik J. Preparation of samples of plant material for chromatographic analysis. *Journal of Chromatographic Science*. 2003;41(3):109–116. 10.1093/chromsci/41.3.109.
12) Krakowska-Sieprawska A, Kiełbasa A, Rafińska K, Ligor M, Buszewski B. Modern methods of pre-treatment of plant material for the extraction of bioactive compounds. *Molecules*. 2022;27(3):730. 10.3390/molecules27030730.
13) Zhang QW, Lin LG, Ye WC. Techniques for extraction and isolation of natural products: A comprehensive review. *Chinese Medicine*. 2018;13(1):20. 10.1186/s13020-018-0177-x.
14) Paragas DS, Cruz KDC, Fiegalan ER. Fermented Azadirachta indica leaves–metal nanoparticles and their insecticidal properties against Bactrocera dorsalis (Hendel). *Indian Journal of Science and Technology*. 2021;14(17):1338–1346. 10.17485/ijst/v14i17.631.

15) Ajaykumar AP, Mathew A, Chandni AP, Varma SR, Jayaraj KN, Sabira O, et al. Green synthesis of silver nanoparticles using the leaf extract of the medicinal plant Uvaria narum and its antibacterial, antiangiogenic, anticancer and catalytic properties. *Antibiotics*. 2023;12(3):564. 10.3390/antibiotics12030564.
16) Ahmed S, Ahmad M, Swami BL, Ikram S. Green synthesis of silver nanoparticles using Azadirachta indica aqueous leaf extract. *Journal of Radiation Research and Applied Sciences*. 2016;9(1):1–7. 10.1016/j.jrras.2015.06.006.
17) Mittal AK, Chisti Y, Banerjee UC. Synthesis of metallic nanoparticles using plant extracts. *Biotechnology Advances*. 2013;31(2):346–356. 10.1016/j.biotechadv.2013.01.003.
18) Shankar SS, Rai A, Ahmad A, Sastry M. Rapid synthesis of Au, Ag, and bimetallic Au core–Ag shell nanoparticles using neem (Azadirachta indica) leaf broth. *Journal of Colloid and Interface Science*. 2004;275(2):496–502. 10.1016/j.jcis.2004.03.003.
19) Iravani S. Green synthesis of metal nanoparticles using plants. *Green Chemistry*. 2011;13(10):2638–2650. 10.1039/C1GC15386B.
20) Song JY, Kim BS. Rapid biological synthesis of silver nanoparticles using plant leaf extracts. *Bioprocess and Biosystems Engineering*. 2009;32(1):79–84. 10.1007/s00449-008-0224-6.
21) Sun Y. Controlled synthesis of colloidal silver nanoparticles in organic solutions: Empirical rules for nucleation engineering. *Chemical Society Reviews*. 2013;42(7):2497–2511. 10.1039/C2CS35289C.
22) Güneş S, Ektiren D, Vardin H. Green synthesis and characterization of silver nanoparticles from Gilaburu under varying temperature and pH, with antimicrobial activity and spectral inconsistencies. *Scientific Reports*. 2025;15(1):38516. 10.1038/s41598-025-00595-1.
23) Miranda A, Akpobolokemi T, Chung E, Ren G, Raimi-Abraham BT. pH alteration in plant-mediated green synthesis and its impact on antimicrobial properties of silver nanoparticles. *Antibiotics*. 2022;11(11):1592. 10.3390/antibiotics11111592.
24) Sunberg RJ. A simple procedure to convert parts per million (ppm) to molarity (M). *Journal of Chemical Education*. 1986;63(8):714. 10.1021/ed063p714.
25) Fahim M, Shahzaib A, Nishat N, Jahan A, Bhat TA, Inam A. Green synthesis of silver nanoparticles: A comprehensive review of methods, influencing factors, and applications. *JCIS Open*. 2024;16:100125. 10.1016/j.jciso.2024.100125.
26) Khuda F, Gul M, Khalil AAK, Ali S, Ullah N, Khan MS, et al. Biosynthesized silver nanoparticles using Alnus nitida leaf extract as a potential antioxidant and anticancer agent. *ACS Omega*. 2023;8(33):30221–30230. 10.1021/acsomega.3c02928.
27) Shahzadi S, Fatima S, Shafiq Z, Janjua MRSA. A review on green synthesis of silver nanoparticles using plant extracts: A multifaceted approach in photocatalysis, environmental remediation, and biomedicine. *RSC Advances*. 2025;15(5):3858–3903. 10.1039/D4RA07519F.
28) He J, Ma Y, Niu X, Pei J, Yan R, Xu F, et al. Silver nanoparticles induce endothelial cytotoxicity through ROS-mediated mitochondrial–lysosomal damage and autophagy perturbation. *Toxicology*. 2024;502:153734. 10.1016/j.tox.2024.153734.
29) Yang T, Yao Q, Cao F, Liu Q, Liu B, Wang XH. Silver nanoparticles inhibit the function of hypoxia-inducible factor-1 and target genes: Insight into cytotoxicity and antiangiogenesis. *International Journal of Nanomedicine*. 2016;p. 6679–6692. 10.2147/IJN.S109695.
30) Yasmeen N, Chaudhary AA, Niraj RRK, Lakhawat SS, Sharma PK, Kumar V. Screening of phytochemicals from Clerodendrum inerme (L.) Gaertn as potential anti-breast cancer compounds targeting EGFR: an in-silico approach. *Journal of Biomolecular Structure and Dynamics*. 2023;43(6):2781–2823. 10.1080/07391102.2023.2294379.
31) Chittasupho C, Samee W, Tadtong S, Jittachai W, Managit C, Athikomkulchai S. Cytotoxicity and apoptosis induction of Clerodendrum chinense flower extract nanoparticles in HeLa cells. *Natural and Life Sciences Communications*. 2023;22(4):e20230. 10.12982/NLSC.2023.057.
32) Chittasupho C, Samee W, Takuathung MN, Okonogi S, Nimkulrat S, Athikomkulchai S. Clerodendrum chinense stem extract and nanoparticles: Effects on proliferation, apoptosis, and mitochondrial membrane potential in breast cancer cells. *International Journal of Molecular Sciences*. 2024;25(2):978. 10.3390/ijms25020978.
33) Chittasupho C, Samee W, Mangmool S, Karuna N, Anuchapreeda S, Okonogi S, et al. Phytochemical characterization and anticancer activity of Clerodendrum chinense leaf extract against breast and cervical cancer cells. *International Journal of Molecular Sciences*. 2025;26(6):2729. 10.3390/ijms26062729.
34) Bhattacharyya S, Samanta S, Hore M, Barai S, Dash SK, Roy S. Phytochemical compositions and biological properties of Clerodendrum thomsoniae leaves. *Pharmacological Research—Natural Products*. 2024;5:100121. 10.1016/j.prenap.2024.100121.
35) Ashraf VK, Kalaichelvan VK, Ragunathan R, Venkatachalam VV. Apoptosis induction and anticancer activity of 2,4-bis(1-phenylethyl) phenol from Clerodendrum thomsoniae in vitro. *International Journal of Pharmaceutical Investigation*. 2020;10(4). 10.5530/ijpi.2020.4.94.
36) Ashraf MVK, Kalaichelvan VK, Ragunathan R, Venkatachalam VV. Antiproliferative potential of Clerodendrum thomsoniae extract on DMBA-induced breast cancer in female Sprague-Dawley rats. *Indian Journal of Pharmaceutical Education and Research*. 2021;55(1):1–10. 10.1186/s43094-021-00206-6.